physics

IMPACT FACTOR 1.8

CITESCORE 3.1

Article

Three-Photon Pulse Interference in a Tritter: A Novel Approach for a Three-Party Quantum Key Distribution Protocol

Suryadi, Precious O. Amadi and Norshamsuri Ali

MDPI

https://doi.org/10.3390/physics7020014

physics

MDPI

Article

Three-Photon Pulse Interference in a Tritter: A Novel Approach for a Three-Party Quantum Key Distribution Protocol

Suryadi [1,*], Precious O. Amadi [2] and Norshamsuri Ali [3]

[1] Computer Engineering Department, Faculty of Engineering, Bina Nusantara (BINUS) University, Jakarta 11480, Indonesia
[2] Institute of Engineering Mathematics, University Malaysia Perlis, Arau Perlis 02600, Malaysia; amadiwati@gmail.com
[3] Faculty of Electronic Engineering Technology, University Malaysia Perlis, Arau Perlis 02600, Malaysia; norshamsuri@unimap.edu.my
* Correspondence: suryadisoekardjo@gmail.com

Abstract: This study presents a theoretical investigation into the interference properties of three photons in a six-port optical beam splitter, commonly referred to as a tritter. We examine various configurations of the relative phase differences among the input photons. Our findings reveal that fully constructive interference periodically occurs at a single output port for specific constant phase differences, while fully destructive interference simultaneously manifests at the remaining two output ports. These distinctive interference patterns arise across a wide range of specific phase difference combinations among the input photons. We suggest that these unique interference characteristics provide new insights into the potential implementation of a three-party quantum key distribution protocol. Such three-photon interference phenomena are crucial for facilitating symmetric secure key distribution among three parties.

Keywords: quantum key distribution (QKD); coherent state; phase-coding QKD; three-photon interference; three-party QKD; tritter

check for updates

Received: 12 November 2024
Revised: 29 March 2025
Accepted: 7 April 2025
Published: 22 April 2025

Citation: Suryadi; Amadi, P.O.; Ali, N. Three-Photon Pulse Interference in a Tritter: A Novel Approach for a Three-Party Quantum Key Distribution Protocol. *Physics* **2025**, *7*, 14. https://doi.org/10.3390/physics7020014

1. Introduction

Photon interference is a captivating phenomenon fundamental to both classical and quantum mechanics. It plays a crucial role in practical technological applications and continues to drive research that expands the understanding of quantum-based technologies. Numerous studies have explored this field, encompassing various aspects of photon interference. These include two-photon interference [1,2], three-photon Hong–Ou–Mandel interference at a three-port device [3], the behavior of a three-path photon interferometer [4], three-photon bosonic interference in an integrated tritter [5], and the coalescence phenomenon in three-photon quantum interferences [6].

Two-photon interference and single-photon interference phenomena have emerged as cornerstone principles in numerous quantum-based technologies. In particular, these phenomena play a pivotal role in the development of two-party quantum key distribution (QKD) protocols. QKD systems generate symmetric encryption keys by leveraging the quantum properties of photons, specifically their phases. Central to this process is the interference of photons within a four-port beam splitter, which serves as a fundamental mechanism in measurement-device-independent QKD (MDI-QKD) [7] and twin-field QKD (TF-QKD) [8].

MDI-QKD [7] is a protocol that addresses all security loopholes on the detection side by introducing an untrusted third party, e.g., Charlie, who performs a two-photon Bell-state

measurement at an intermediate node. Since its inception, MDI-QKD has achieved numerous theoretical and experimental breakthroughs [9–16]. TF-QKD [8] is an innovative protocol considered a promising solution for long-distance QKD, capable of surpassing the repeaterless bound using current technologies. In this protocol, an intermediate node, Charlie, measures the first-order interference of two optical fields originating from Alice and Bob. The original TF-QKD protocol has inspired numerous variants, including theoretical studies [11,17–21], practical designs [11,17,22,23], and experimental demonstrations [23–27].

A three-party quantum secret sharing (QSS) protocol utilizing multipartite entangled states—specifically Greenberger–Horne–Zeilinger (GHZ) entangled states—known as QSS—was first introduced in ref. [28]. Following this pioneering paper, significant advancements in QSS based on multipartite entanglement have led to the development of numerous variants. These include innovations in both theory and experimental implementation, as demonstrated in recent studies [29–34], reflecting the growing interest and progress in this field. Many QSS protocols utilizing GHZ entangled states require complex GHZ or Bell state measurements, adding to the technical challenges of implementation.

Initially, TF-QKD protocols utilized a relatively simple measurement system based on two-photon pulse interference in a 2×2 beam splitter. However, these protocols were primarily limited to two-party systems. In contrast, QSS protocols were proposed for three-party QKD systems but required complex measurements involving GHZ or Bell states. These limitations have prompted the investigation in this paper into three-photon pulse interference in a tritter, with a particular focus on varying input phase modulations. This approach shows promise as a simplified measurement device for three-photon QKD protocols. To this end, we theoretically explore three-photon pulse interference in a three-dimensional integrated six-port optical beam splitter (tritter). Our tritter design features independently and continuously adjustable phase modulators at each input port. We model the tritter as an ideal, lossless, and symmetric six-port beam splitter. By simultaneously injecting indistinguishable weak coherent photon pulses of equal amplitude into all three input ports, we demonstrate precise control over the output photon distribution probabilities (i.e., one, two, or three photons per output port) through specific phase differences among the input photons. A notable phenomenon observed in this system is periodic coalescence, where, at specific phase differences, all photons converge into a single output port. This unique interference pattern provides a promising foundation for a simplified measurement system in three-party phase-coding QKD protocols.

2. Three Coherent Photons' Interference at a Tritter

2.1. Unitary Matrices of the Tritter and Phase Modulator

A tritter [35,36] is a 3×3 integrated optical coupler that enables coherent splitting and mixing of optical signals across three spatial modes, functioning as a three-mode analog of a beam splitter. Its optical propagation dynamics are governed by specific coupling coefficients and phase relationships. Conventional approaches to multi-mode optical processing rely on the Reck [37] and Clements [38] decomposition models, which decompose larger unitary matrices into cascades of 2×2 transformations using beam splitters. While the Reck model employs a stepwise diagonalization process, the Clements design optimizes spatial arrangement for enhanced stability and loss tolerance. However, these decomposition-based implementations demand numerous optical elements, constraining scalability. An alternative approach involves the use of integrated optical devices such as the tritter, a 3×3 optical coupler that enables three-way photon splitting through evanescent wave interactions in integrated waveguide structures [5,39,40]. The transformation matrix of a tritter derives from coupled-mode equations, with coupling strength and propagation constants determining photon distribution across output ports. Unlike beam splitter networks,

tritters provide a compact and efficient platform for realizing higher-dimensional unitary operations, substantially reducing hardware complexity while preserving coherence.

In this study, we focus on an ideal, symmetric tritter, modeled as a three-dimensional integrated beam splitter. This device consists of a directional coupler in which three waveguides are closely aligned and coupled through evanescent fields [5]. In a symmetric tritter configuration, the coupling coefficients among the three waveguides are equal. Consequently, a single photon entering any input port has an equal probability of exiting from any of the three output ports.

Figure 1 depicts a tritter model with photon phase modulators integrated into each input port, as analyzed in this paper. The unitary operator for the ideal, lossless, and symmetric directional coupler-based tritter (six-port beam splitter) is given as follows [40]:

$$U_{\mathrm{T}} = \sqrt{\frac{1}{3}} \begin{pmatrix} 1 & e^{i\frac{2\pi}{3}} & e^{i\frac{2\pi}{3}} \\ e^{i\frac{2\pi}{3}} & 1 & e^{i\frac{2\pi}{3}} \\ e^{i\frac{2\pi}{3}} & e^{i\frac{2\pi}{3}} & 1 \end{pmatrix}. \tag{1}$$

The unitary operator for the phase modulator in Figure 1 is given as follows:

$$U_{\varphi} = \begin{pmatrix} e^{-i\varphi_1} & 0 & 0 \\ 0 & e^{-i\varphi_2} & 0 \\ 0 & 0 & e^{-i\varphi_3} \end{pmatrix}, \tag{2}$$

where φ_j is the relative phase shift at input port j with $j = 1, 2,$ or 3. We investigate the interference pattern of weak coherent pulses in a tritter, equipped with phase modulators on each input port, as a potential platform for three-party QKD.

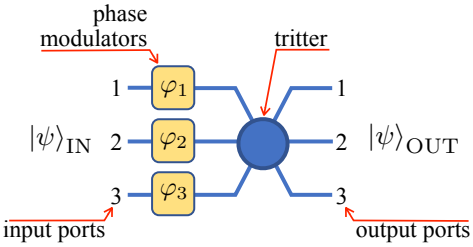

Figure 1. Schematic of the tritter model, a symmetric six-port beam splitter (tritter) with continuously tunable phase modulators at each input port. The input coherent photon state and output state are represented as $|\psi\rangle_{\mathrm{IN}}$ and $|\psi\rangle_{\mathrm{OUT}}$, respectively.

2.2. Input Photon States

Weak coherent pulses provide a balance between practicality and security, making them a suitable choice for current QKD systems. Although single-photon sources hold the potential to offer enhanced security, weak coherent pulses remain the dominant technology due to their ease of implementation and cost-effectiveness.

A coherent state $|\alpha\rangle$, also called Glauber state, is defined as an eigenstate of the annihilation operator $\hat{a}$, satisfying $\hat{a}|\alpha\rangle = \alpha|\alpha\rangle$ [41,42]. Here, $\alpha = |\alpha|\exp(i\varphi) \in \mathbb{C}$ is a complex number and $\hat{a}$ is an annihilation operator. The phase φ in α describes the wave aspect of the coherent state $|\alpha\rangle$. The particle-like aspect of the coherent state can be understood by expressing it as a superposition of Fock states with indefinite photon numbers. Using the completeness relation of the Fock states $|n\rangle$, the coherent state $|\alpha\rangle$ can be written as

$$|\alpha\rangle = \exp\left(-\frac{|\alpha|^2}{2}\right) \sum_{n=0}^{\infty} \frac{\alpha^n}{\sqrt{n!}} |n\rangle, \tag{3}$$

where $|n\rangle$ denotes the photon-number (Fock) state containing n photons. The statistical model of the coherent state, as described by Equation (3), exhibits a Gaussian profile and follows a Poisson distribution. Consequently, the probability of emitting n photons in a coherent state is given by $P(n) = e^{-\mu}\mu^n/n!$, where $\mu = |\alpha|^2$ represents the average photon number per pulse.

In Figure 1, the tritter model investigated in this study uses weak coherent photon states (3) as inputs for each port. Thus, the input photon states for the tritter system can be expressed as

$$\begin{aligned} |\psi\rangle_{\text{IN}} &= |\alpha_1\rangle|\alpha_2\rangle|\alpha_3\rangle \\ &= \prod_{i=1}^{3}\sum_{n=0}^{\infty}\exp\left(-\frac{|\alpha_i|^2}{2}\right)\frac{\alpha_i^{n_i}}{\sqrt{n_i!}}|n_i\rangle, \end{aligned} \tag{4}$$

where $|\alpha_1\rangle$, $|\alpha_2\rangle$, and $|\alpha_3\rangle$ represent the coherent photon states (3) injected into input ports 1, 2, and 3, respectively.

2.3. Output Photon States

When three coherent photons, as described in Equation (4), are injected into the ports of the tritter system (illustrated in Figure 1), which is equipped with independent phase modulators at each input port, the resulting output photon state can be determined by

$$|\psi\rangle_{\text{OUT}} = \hat{U}_T\hat{U}_\varphi|\psi\rangle_{\text{IN}}, \tag{5}$$

where $\hat{U}_T$ and $\hat{U}_\phi$ represent the unitary matrices for the tritter (1) and the phase modulator (2), respectively. $|\psi\rangle_{\text{IN}}$ denotes the input coherent photon state given by Equation (4). By solving Equation (5), one obtains the output photon state from the tritter as

$$|\psi\rangle_{\text{OUT}} = \prod_{i=1}^{3}\sum_{n=0}\exp\left(-\frac{|\zeta_i|^2}{2}\right)\frac{\zeta_i^{n_i}}{\sqrt{n_i!}}|n_i\rangle, \tag{6}$$

where

$$\begin{aligned} \zeta_1 &= \frac{1}{\sqrt{3}}[\alpha_1 e^{-i\varphi_1} + e^{i\frac{2\pi}{3}}(\alpha_2 e^{-i\varphi_2} + \alpha_3 e^{-i\varphi_3})], \\ \zeta_2 &= \frac{1}{\sqrt{3}}[\alpha_2 e^{-i\varphi_2} + e^{i\frac{2\pi}{3}}(\alpha_1 e^{-i\varphi_1} + \alpha_3 e^{-i\varphi_3})], \\ \text{and}\quad \zeta_3 &= \frac{1}{\sqrt{3}}[\alpha_3 e^{-i\varphi_3} + e^{i\frac{2\pi}{3}}(\alpha_1 e^{-i\varphi_1} + \alpha_2 e^{-i\varphi_2})]. \end{aligned} \tag{7}$$

For the special case of indistinguishable input photons, the output photon state (6) explicitly shows that three-photon interference in the tritter is governed exclusively by the relative phase differences among the input photon states, denoted by φ_1, φ_2, and φ_3.

2.4. Probability Distribution Output Photons

As discussed in Section 2.1, our calculations employ a model of a lossless and symmetrical tritter, specifically examining the case where indistinguishable photon states are injected into the input ports. Under these conditions, we calculated the probability distribution of output photons as a function of the relative phase differences between the input photon states, as shown in Figure 2, which presents three scenarios.

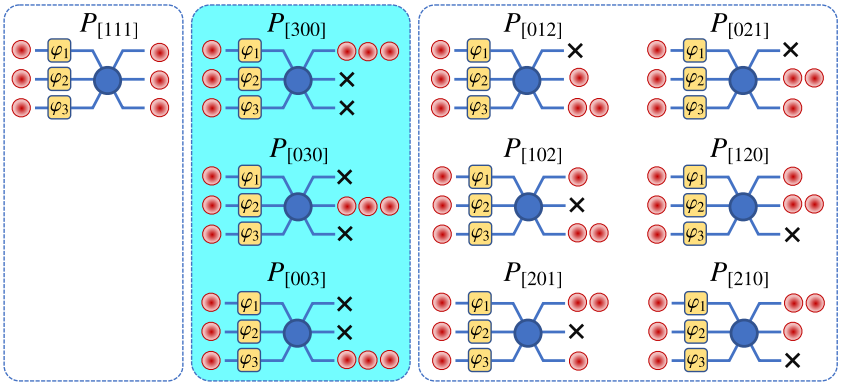

Figure 2. Probability distribution of the output photons as a function of the relative phase differences among the input photon states for the three distinct scenarios: (**left**) photons (red dots) are uniformly distributed across all three output ports with equal probability; (**middle**) all three photons coalesce into a single output port; and (**right**) when one output port registers no photons (crosses), the remaining two ports exhibit an asymmetric distribution of the three photons.

We then proceed to calculate the probability for each photon distribution shown in Figure 2. The output photon number state representation (6) can be expressed as a coherent state with a Poisson distribution of photons. This can be mathematically formulated as

$$P_{[n_1 n_2 n_3]} = \left|\langle n_1 n_2 n_3|\psi\rangle_{\mathrm{OUT}}\right|^2, \tag{8}$$

where n_1, n_2, and n_3 denote the number of photons detected at output ports 1, 2, and 3, respectively. The values of n_1, n_2, and n_3 may be 0, 1, 2, or 3, subject to the conservation condition $n_1 + n_2 + n_3 = 3$. The probability of photons being equally distributed among all three output ports was calculated and obtained as

$$P_{[111]} = \left|\langle 111|\psi\rangle_{\mathrm{OUT}}\right|^2 = \exp\left(-\sum_{i=1}^{3}|\zeta_i|^2\right)\prod_{i=1}^{3}\frac{|\zeta_i|^2}{3!}. \tag{9}$$

The probability distributions for the photon state to be coalesced at one of the output ports are given by

$$P_{[300]} = \left|\langle 300|\psi\rangle_{\mathrm{OUT}}\right|^2 = \exp\left(-\sum_{i=1}^{3}|\zeta_i|^2\right)\frac{|\zeta_1|^2}{3!}, \tag{10}$$

$$P_{[030]} = \left|\langle 030|\psi\rangle_{\mathrm{OUT}}\right|^2 = \exp\left(-\sum_{i=1}^{3}|\zeta_i|^2\right)\frac{|\zeta_2|^2}{3!}, \tag{11}$$

$$P_{[003]} = \left|\langle 003|\psi\rangle_{\mathrm{OUT}}\right|^2 = \exp\left(-\sum_{i=1}^{3}|\zeta_i|^2\right)\frac{|\zeta_3|^2}{3!}. \tag{12}$$

The photon distribution for the scenario where one of the output ports has no detected photons, and the other two output ports detect three photons unequally, is characterized by the probability of

$$P_{[012]} = \left|\langle 012|\psi\rangle_{\mathrm{OUT}}\right|^2 = \exp\left(-\sum_{i=1}^{3}|\zeta_i|^2\right)\frac{|\zeta_2|^2|\zeta_3|^4}{2!}, \tag{13}$$

$$P_{[021]} = \left|\langle 021|\psi\rangle_{\mathrm{OUT}}\right|^2 = \exp\left(-\sum_{i=1}^{3}|\zeta_i|^2\right)\frac{|\zeta_2|^4|\zeta_3|^2}{2!}, \tag{14}$$

$$P_{[102]} = \left|\langle 102|\psi\rangle_{\mathrm{OUT}}\right|^2 = \exp\left(-\sum_{i=1}^{3}|\zeta_i|^2\right)\frac{|\zeta_1|^2|\zeta_3|^4}{2!}, \tag{15}$$

$$P_{[120]} = \left|\langle 120|\psi\rangle_{\mathrm{OUT}}\right|^2 = \exp\left(-\sum_{i=1}^{3}|\zeta_i|^2\right)\frac{|\zeta_1|^2|\zeta_2|^4}{2!}, \tag{16}$$

$$P_{[201]} = \left|\langle 201|\psi\rangle_{\mathrm{OUT}}\right|^2 = \exp\left(-\sum_{i=1}^{3}|\zeta_i|^2\right)\frac{|\zeta_1|^4|\zeta_3|^2}{2!}, \tag{17}$$

$$P_{[210]} = \left|\langle 210|\psi\rangle_{\mathrm{OUT}}\right|^2 = \exp\left(-\sum_{i=1}^{3}|\zeta_i|^2\right)\frac{|\zeta_1|^4|\zeta_2|^2}{2!}, \tag{18}$$

with the parameters ζ_i $(i = 1, 2, 3)$ defined in Equation (7).

2.5. Interference Fringes

The analysis focuses on the coalescence condition where all three input photons merge into a single output port. To visualize the probability of detecting output photons, we plot Equations (10)–(12) using Mathematica (version 13.3) in Figure 3 which illustrates the results corresponding to Equation (10), depicting the probability $P_{[300]}$ of detecting an output photon at port 1. The probability is plotted as a function of the phase differences φ_2 and φ_3 between the input photons at ports 2 and 3, respectively, over one complete period, ranging from 0 to 2π rad. The phase difference φ_1 of the input photon at port 1 is fixed at periodic values of $2\pi/3, \pi, 4\pi/3, 5\pi/3, 0$, and $\pi/3$ rad.

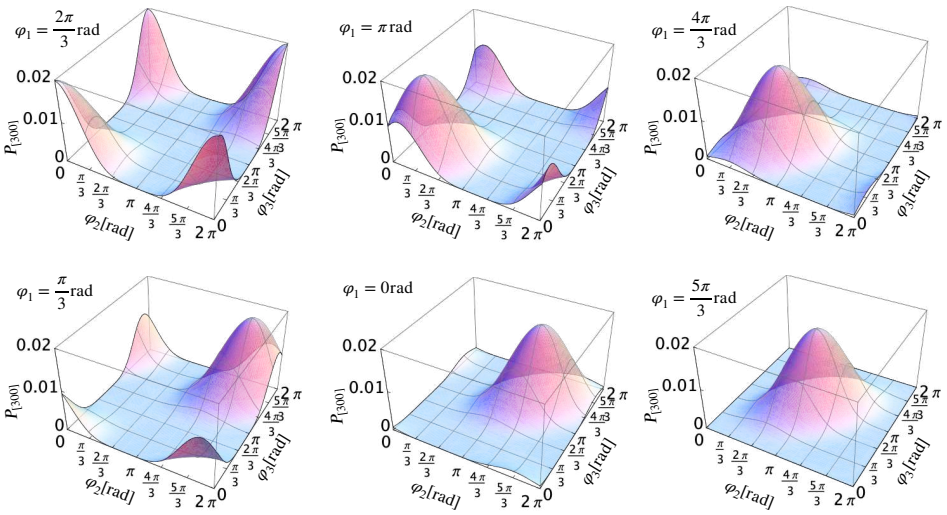

Figure 3. Detection probability of an output photon at port 1 ($P_{[300]}$ (10)) against the phase differences φ_2 and φ_3 of input photons at ports 2 and 3, respectively, for various fixed phase difference φ_1 values of the input photon at port 1 as indicated. The average photon number per pulse (μ) for all three input ports was set to 0.2.

As shown in Figure 3, the observed interference patterns indicate that all photons periodically converge to a single output port, contingent on the specific phase relationships among the input photons. Table 1 summarizes these phase difference combinations for

maximum probabilities of the ditribution $P_{[300]}$. Notably, the $|111\rangle$ input photon state exclusively converges to output port 1 when photons at ports 2 and 3 share the same relative phase. Similar probability distributions were obtained for output ports 2 and 3, $P_{[030]}$ (11)and $P_{[003]}$ (12), respectively (not shown).

Table 1. The phase differences combinations for maximum probabilities Author: Yes, this correct. at output port 1 ($P_{[300]}$ (10)), occurring for specific values of the relative phase differences φ_1 of input photons at port 1.

φ_1	0	$\frac{\pi}{3}$	$\frac{2\pi}{3}$	π	$\frac{4\pi}{3}$	$\frac{5\pi}{3}$
φ_2	$\frac{4\pi}{3}$	$\frac{5\pi}{3}$	0	$\frac{\pi}{3}$	$\frac{2\pi}{3}$	π
φ_3	$\frac{4\pi}{3}$	$\frac{5\pi}{3}$	0	$\frac{\pi}{3}$	$\frac{2\pi}{3}$	π

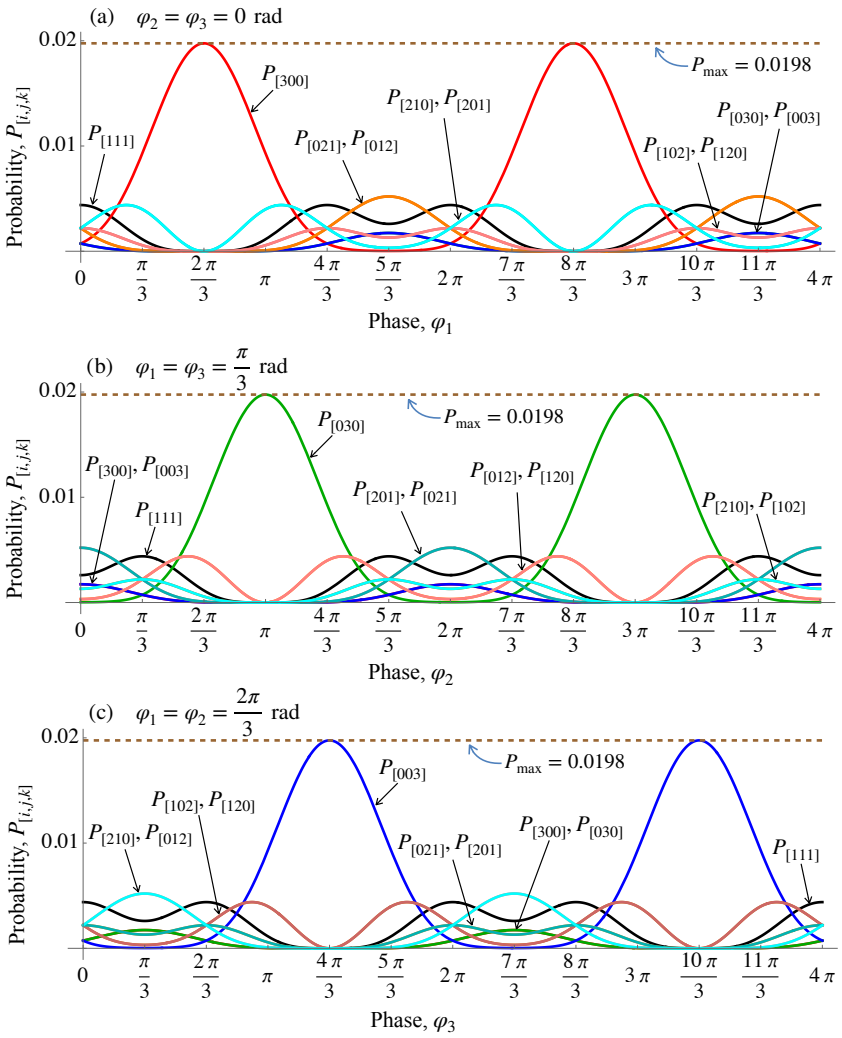

Figure 4. Probability distribution of photons, $P_{[ijk]}$ (9), (10)–(12) and (13)–(18) as a function of the relative phase difference φ_1 (**a**), φ_2 (**b**), and φ_3 (**c**) at fixed values of the other two relative phase differences as indicated. The dashed horizontal line at $P_{\max} = 0.0198$ represents the maximum detection probability of the non-empty pulse, calculated by summing all probability distributions (9), (10)–(12) and (13)–(18). The average photon number per pulse (μ) for all three input ports was set to 0.2.

To further investigate the photon coalescence condition, where all photons converge into a single output port with maximum probabilities of the distributions (10)–(12), we analyze all

probability distributions including the distributions (9) and (13)–(18). Figure 4 shows the probability distributions $P_{[ijk]}$ of photons as a function of the relative phase differences φ_1 (Figure 4a), φ_2 (Figure 4b), and φ_3 (Figure 4c), while keeping the other two relative phase differences fixed. The results obtained demonstrate that all maximum peaks for all coalescence conditions are tangent to the maximum probability line, further confirming that under these conditions, all photons converge to a single output port.

Complete photon coalescence into a single output port— port 1 ($P_{[300]}$), port 2 ($P_{[030]}$), or port 3 ($P_{[003]}$)—occurs only for specific relative input photon phase differences, as detailed in Table 2. The maximum probability at port 1 ($P_{[300]}$) is achieved when phases φ_2 and φ_3 are synchronized and both lag behind φ_1 by $\frac{2}{3}\pi$. For port 2 ($P_{[030]}$), the probability peaks when φ_1 and φ_3 are in phase, lagging behind φ_2 by $\frac{2}{3}\pi$. Similarly, port 3 ($P_{[003]}$) reaches maximum probability when φ_1 and φ_2 are synchronized, lagging behind φ_3 by $\frac{2}{3}\pi$. These results indicate that under conditions of complete constructive interference, the photon probability distributions at port 1 ($P_{[300]}$), port 2 ($P_{[030]}$), and port 3 ($P_{[003]}$) reach their maximum values through a multitude of distinct phase combinations. This distinctive interference pattern presents a promising approach for implementing symmetric distance protocols in three-party QKD systems.

Table 2. Combination of the relative phase difference of the input photons to obtain the maximum probability distribution at output port 1, 2, and 3.

Probability	Phase φ_1	Phase φ_2	Phase φ_3	P_{max} ‡
$P_{[300]}$	$(\phi_i$ † $+ \frac{2\pi}{3})$	ϕ_i	ϕ_i	1.98%
$P_{[030]}$	ϕ_j †	$(\phi_j + \frac{2\pi}{3})$	ϕ_j	1.98%
$P_{[003]}$	ϕ_k †	ϕ_k	$(\phi_k + \frac{2\pi}{3})$	1.98%

† The phases ϕ_i, ϕ_j, and ϕ_k may be assigned arbitrary values in radians. ‡ The probability maximum (P_{max}) was calculated with the average photon number per pulse (μ) set to 0.2 for all three input ports.

3. Possible Applications for a Three-Party Quantum Key Distribution Protocol

Drawing inspiration from the significant advancements in QKD protocols—MDI-QKD [7], TF-QKD [8], and QSS [28]—we propose a novel approach for three-party QKD implementations. The TF-QKD protocol establishes a two-party framework that leverages weak coherent pulse interference to generate symmetric keys through a simplified measurement system. In contrast, the QSS protocol extends to three parties but relies on relatively complex GHZ or Bell state measurements to distribute symmetric keys. The current study focuses on the interference of three-photon pulses in a tritter with precisely controlled input photon phases. This approach aims to bridge the gap in developing three-party protocol configurations that maintain measurement simplicity while expanding the participant capacity. By doing so, one seeks to enhance the scalability and practicality of multi-party QKD systems.

Figure 5 presents a preliminary conceptual framework for a three-party QKD implementation, which requires further refinement to establish a complete and detailed protocol. In this configuration, three parties—Alice, Bob, and Charlie—are each equipped with identical weak coherent photon pulse generators and phase modulators at their respective transmitter stations. These stations are positioned equidistant from a central measurement station operated by Dave, which is equipped with a tritter and single-photon detectors. We propose that photon interference within the tritter represents a promising candidate for implementing a three-party QKD protocol, enabling secure key distribution through interference pattern analysis. A potential scenario in which phase-dependent interference in a tritter enables a three-party QKD protocol is outlined in the following key procedures.

1. Alice, Bob, and Charlie independently generate weak coherent states using their respective laser sources (LSs), represented as $\left|\alpha e^{(\frac{\pi}{3N})x}\right\rangle$, $\left|\alpha e^{(\frac{\pi}{3N})y}\right\rangle$, and $\left|\alpha e^{(\frac{\pi}{3N})z}\right\rangle$, respectively, where $x, y, z \in \{0, 1, 2, \ldots, N-1\}$ are randomly chosen by Alice, Bob, and Charlie. Here, to ensure that the combined random phases adhere to the rule outlined in Table 2, the phases chosen by Alice, Bob, and Charlie are discretized in increments of $\pi/3N$, where N is an integer.
2. Alice, Bob, and Charlie simultaneously send their quantum states to an untrusted measurement station, Dave. Dave performs three-photon interference measurements using a tritter (a six-port optical beam splitter) and single-photon detectors D_0, D_1, and D_2. For each trial, the following six outcomes are possible: "Only D_0 clicks", "Only D_1 clicks", "Only D_2 clicks", "All detectors click", "Two detectors click", and "No detectors click". By considering the cases where "All detectors click", "Two detectors click", or "No detectors click" as "No clicks", Dave announces one of four possible outcomes.
3. Following the detection and announcement session, Alice, Bob, and Charlie can identify the successful detection outcomes ("Only D_0 clicks", "Only D_1 clicks", and "Only D_2 clicks",) that correlate with their randomly selected phase values x, y, and z. These outcomes are classified according to the following conditions: "Only D_0 clicks" when $y = z$, "Only D_1 clicks" when $x = z$, and "Only D_2 clicks" when $x = y$. Based on these distinctive detection pattern characteristics in conjunction with their random phase combinations, one expects that raw keys can be established through further exploration.

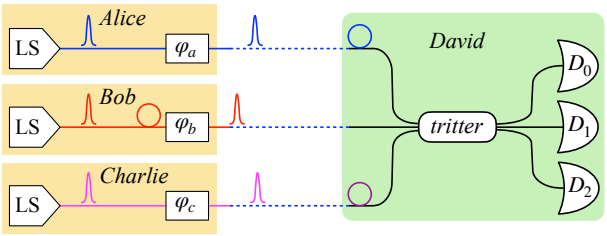

Figure 5. The schematic of the main portion of the proposed initial framework of the three-party quantum key distribution (QKD) protocol involves three laser source (LS) transmitters—Alice, Bob, and Charlie (yellow area)—and a central measurement station operated by Dave (green area). Each transmitter is equipped with identical weak photon pulse generators and phase modulators. Alice, Bob, and Charlie individually prepare optical pulses with random phases φ_a, φ_b, and φ_c, respectively, which they encode and transmit through the quantum channel. Dave's central station employs a tritter to overlap the input pulses and measures them using single-photon detectors D_0, D_1, and D_2. The peaks represent the coherent laser pulses, and the loops correspond to the adjustable optical delay line enabling pulse synchronization at the tritter.

The QKD framework describes our initial exploration into a three-party quantum key distribution protocol that utilizes a comparatively simple measurement system. While we have established the foundational concept, substantial research remains necessary to refine the protocol, including developing robust coding systems, formal security proofs, error correction mechanisms, and privacy amplification techniques.

4. Conclusions

In conclusion, our study provides a theoretical investigation of three-photon interference in a lossless, symmetrical tritter—a six-port beam splitter—equipped with continuously and independently adjustable phase modulators at each input port. We introduced indistinguishable photon states simultaneously and equally into all three input ports and

identified a coalescence condition in which all photons converged at a single output port. This interference phenomenon occurred when the relative phase difference between one input photon and the others was precisely $2\pi/3$ rad, while the remaining two phases were equal. The observed interference patterns arise from a specific set of phase difference combinations among the input photons. Building on this unique interference behavior, we propose a potential application for a three-party quantum key distribution (QKD) protocol. While this work establishes a foundational element for the three-party QKD framework, further research is required to fully develop the protocol and address the practical implementation challenges. This study lays the groundwork for future advancements in multi-photon interference-based quantum communication systems.

Author Contributions: Conceptualization, methodology, formal analysis, and writing—original draft preparation, S.; validation, S., P.O.A. and N.A.; writing—review and editing, P.O.A. and N.A.; supervision, N.A.; funding acquisition, S. and N.A. All authors have read and agreed to the published version of the manuscript.

Funding: This research was financially supported by the Directorate of Research and Community Service, Ministry of Higher Education, Science, and Technology, Republic of Indonesia through the Fundamental Research scheme, grant numbers 105/E5/PG.02.00.PL/2024, 784/LL3/AL.04/2024, and 092/VRRTT/VI/2024.

Data Availability Statement: The original contributions presented in the study are included in the article.

Acknowledgments: We thank the Unit Research and Technology Transfer Office, Bina Nusantara (BINUS) University, Indonesia, for providing facilities and partial financial support.

Conflicts of Interest: The authors declare no conflicts of interest.

References

1. Hong, C.K.; Ou, Z.Y.; Mandel, L. Measurement of subpicosecond time intervals between two photons by interference. *Phys. Rev. Lett.* **1987**, *59*, 2044–2046. [CrossRef]
2. Bouchard, F.; Sit, A.; Zhang, Y.; Fickler, R.; Miatto, F.M.; Yao, Y.; Sciarrino, F.; Karimi, E. Two-photon interference: The Hong–Ou–Mandel effect. *Rep. Prog. Phys.* **2020**, *84*, 012402. [CrossRef]
3. Mährlein, S.; von Zanthier, J.; Agarwal, G.S. Complete three photon Hong–Ou–Mandel interference at a three port device. *Opt. Express* **2015**, *23*, 15833–15847. [CrossRef]
4. Yuan, Q.; Feng, X. Three-path interference of a photon and reexamination of the nested Mach–Zehnder interferometer. *Phys. Rev. A* **2019**, *99*, 053805. [CrossRef]
5. Spagnolo, N.; Vitelli, C.; Aparo, L.; Mataloni, P.; Sciarrino, F.; Crespi, A.; Ramponi, R.; Osellame, R. Three-photon bosonic coalescence in an integrated tritter. *Nat. Commun.* **2013**, *4*, 1606. [CrossRef]
6. Ripala, D.P.; Rohedi, A.Y.; Suryadi. Coalescence Phenomenon in the three photon quantum interferences. *J. Phys. Conf. Ser.* **2021**, *1821*, 012046. [CrossRef]
7. Lo, H.-K.; Curty, M.; Qi, B. Measurement-device-independent quantum key distribution. *Phys. Rev. Lett.* **2012**, *108*, 130503. [CrossRef]
8. Lucamarini, M.; Yuan, Z.L.; Dynes, J.F.; Shields, A.J. Overcoming the rate–distance limit of quantum key distribution without quantum repeaters. *Nature* **2018**, *557*, 400–403. [CrossRef]
9. Fu, Y.; Yin, H.-L.; Chen, T.-Y.; Chen, Z.-B. Long-distance measurement-device-independent multiparty quantum communication. *Phys. Rev. Lett.* **2015**, *114*, 090501. [CrossRef]
10. Yin, H.-L.; Chen, T.-Y.; Yu, Z.-W.; Liu, H.; You, L.-X.; Zhou, Y.-H.; Chen, S.-J.; Mao, Y.; Huang, M.-.Q.; Zhang, W.-J.; et al. Measurement-device-independent quantum key distribution over a 404 km optical fiber. *Phys. Rev. Lett.* **2016**, *117*, 190501. [CrossRef]
11. Cui, Z.-X.; Zhong, W.; Zhou, L.; Sheng, Y.-B. Measurement-device-independent quantum key distribution with hyper-encoding. *Sci. China Phys. Mech. Astron.* **2019**, *62*, 110311. [CrossRef]
12. Hu, L.-W.; Zhang, C.-M.; Li, H.-W. Practical measurement-device-independent quantum key distribution with advantage distillation. *Quant. Inform. Process.* **2023**, *22*, 77. [CrossRef]

13. Wang, X.; Lu, F.-Y.; Wang, Z.-H.; Yin, Z.-Q.; Wang, S.; Geng, J.-Q.; Chen, W.; He, D.-Y.; Guo, G.-C.; Han, Z.-F. Fully passive measurement-device-independent quantum key distribution. *Phys. Rev. Appl.* **2024**, *21*, 064067. [CrossRef]
14. Xie, Y.-M.; Bai, J.-L.; Lu, Y.-S.; Weng, C.-X.; Yin, H.-L.; Chen, Z.-B. Advantages of asynchronous measurement-device-independent quantum key distribution in intercity networks. *Phys. Rev. Appl.* **2023**, 19, 054070. [CrossRef]
15. Zhang, K.; Liu, J.; Ding, H.; Zhou, X.; Zhang, C.; Wang, Q. Asymmetric measurement-device-independent quantum key distribution through advantage distillation. *Entropy* **2023**, *25*, 1174. [CrossRef]
16. Kang, G.-D.; Liu, J.; Zhang, T.; Zhou, Q.-P.; Fang, M.-F. Fully measurement-device-independent two-way quantum key distribution with finite single-photon sources. *Quant. Inform. Process.* **2024**, *23*, 211. [CrossRef]
17. Wang, X.-B.; Yu, Z.-W.; Hu, X.-L. Twin-field quantum key distribution with large misalignment error. *Phys. Rev. A* **2018**, *98*, 062323. [CrossRef]
18. Curty, M.; Azuma, K.; Lo, H.-K. Simple security proof of twin-field type quantum key distribution protocol. *npj Quant. Inform.* **2019**, *5*, 64. [CrossRef]
19. Qian, X.; Zhang, C.; Yuan, H.; Zhou, X.; Li, J.; Wang, Q. Passive light source monitoring for sending or not sending twin-field quantum key distribution. *Entropy* **2022**, *24*, 592. [CrossRef]
20. Xue, K.; Shen, Z.; Zhao, S.; Mao, Q. Sending-or-not-sending twin-field quantum key distribution with a passive decoy-state method. *Entropy* **2022**, *24*, 662. [CrossRef]
21. Krawec, W.O. A New security proof for twin-field quantum key distribution (QKD). *Appl. Sci.* **2024**, *14*, 187. [CrossRef]
22. Yin, H.-L.; Fu, Y. Measurement-device-independent twin-field quantum key distribution. *Sci. Rep.* **2019**, *9*, 3045. [CrossRef]
23. Bertaina, G.; Clivati, C.; Donadello, S.; Liorni, C.; Meda, A.; Virzì, S.; Gramegna, M.; Genovese, M.; Levi, F.; Calonico, D.; et al. Phase noise in real-world twin-field quantum key distribution. *Adv. Quant. Technol.* **2024**, *7*, 2400032. [CrossRef]
24. Chen, J.-P.; Zhang, C.; Liu, Y.; Jiang, C.; Zhang, W.-J.; Han, Z.-Y.; Ma, S.-Z.; Hu, X.-L.; Li, Y.-H.; Liu, H.; et al. Twin-field quantum key distribution over a 511 km optical fibre linking two distant metropolitan areas. *Nat. Photonics* **2021**, *15*, 570–575. [CrossRef]
25. Pittaluga, M.; Minder, M.; Lucamarini, M.; Sanzaro, M.; Woodward, R.I.; Li, M.-J.; Yuan, Z.; Shields, A.J. 600-km repeater-like quantum communications with dual-band stabilization. *Nat. Photonics* **2021**, *15*, 530–535. [CrossRef]
26. Chen, J.P.; Zhang, C.; Liu, Y.; Jiang, C.; Zhang, W.; Hu, X.L.; Guan, J.-Y.; Yu, Z.-W.; Xu, H.; Lin, J.; et al. Sending-or-not-sending with independent lasers: Secure twin-field quantum key distribution over 509 km. *Phys. Rev. Lett.* **2020**, *124*, 070501. [CrossRef]
27. Liu, H.; Jiang, C.; Zhu, H.-T.; Zou, M.; Yu, Z.W.; Hu, X.-L.; Xu, H.; Ma, S.; Han, Z.; Chen, J.P.; et al. Field test of twin-field quantum key distribution through sending-or-not-sending over 428 km. *Phys. Rev. Lett.* **2021**, *126*, 250502. [CrossRef]
28. Hillery, M.; Bužek, V.; Berthiaume, A. Quantum secret sharing. *Phys. Rev. A* **1999**, *59*, 1829–1834. [CrossRef]
29. Zhou, R.-G.; Huo, M.; Hu, W.; Zhao, Y. Dynamic multiparty quantum secret sharing with a trusted party based on generalized GHZ state. *IEEE Access* **2021**, *19*, 22986–22995. [CrossRef]
30. Li, C.-L.; Fu, Y.; Liu, W.-B.; Xie, Y.-M.; Li, B.-H.; Zhou, M.-G.; Yin, H.-L.; Chen, Z.-B. Breaking the rate-distance limitation of measurement-device-independent quantum secret sharing. *Phys. Rev. Res.* **2023**, *5*, 033077. [CrossRef]
31. Cai, X.-Q.; Li, S.; Liu, Z.-F.; Wang, T.-Y. Measurement-device-independent quantum secret sharing. *Adv. Quant. Technol.* **2024**, *7*, 2400060. [CrossRef]
32. Zhang, Q.; Ying, J.-W.; Wang, Z.-J.; Zhong, W.; Du, M.-M.; Shen, S.-T.; Li, X.-Y.; Zhang, A.-L.; Gu, S.-P.; Wang, X.-F.; et al. Device-independent quantum secret sharing with advanced random key generation basis. *Phys. Rev. A* **2025**, *111*, 012603. [CrossRef]
33. Liu, S.; Lu, Z.; Wang, P.; Tian, Y.; Wang, X.; Li, Y. Experimental demonstration of multiparty quantum secret sharing and conference key agreement. *npj Quant. Inform.* **2023**, *9*, 92. [CrossRef]
34. Zhang, Q.; Zhong, W.; Du, M.-M.; Shen, S.-T.; Li, X.-Y.; Zhang, A.-L.; Zhou, L.; Sheng, Y.-B. Device-independent quantum secret sharing with noise preprocessing and postselection. *Phys. Rev. A* **2024**, *110*, 042403. [CrossRef]
35. Zeilinger, A.; Bernstein, H.J.; Greenberger, D.M.; Horne, M.A.; Zukowski, M. Controlling entanglement in quantum optics; In *Quantum Control and Measurement*; Ezawa, H.; Murayama, Y., Eds.; North-Holland/Elsevier Science Publishers B.V.: Amsterdam, The Netherlands, 1993; pp. 9–23. Available online: https://www.researchgate.net/publication/253722501_Controlling_entanglement_in_quantum_optics (accessed on 4 April 2025).
36. Osawa, S.; Simon, D.S.; Sergienko, A.V. Directionally-unbiased unitary optical devices in discrete-time quantum walks. *Entropy* **2019**, *21*, 853. [CrossRef]
37. Reck, M.; Zeilinger, A.; Bernstein, H.J.; Bertani, P. Experimental realization of any discrete unitary operator. *Phys. Rev. Lett.* **1994**, *73*, 58–61. [CrossRef]
38. Clements, W.R.; Humphreys, P.C.; Metcalf, B.J.; Kolthammer, W.S.; Walmsley, I.A. Optimal design for universal multiport interferometers. *Optica* **2016**, *3*, 1460–1465. [CrossRef]
39. Meany, T.; Delanty, M.; Gross, S.; Marshall, G.D.; Steel, M.J.; Withford, M.J. Non-classical interference in integrated 3D multiports. *Opt. Express* **2012**, *20*, 26895–26905. [CrossRef]

40. Spagnolo, N.; Aparo, L.; Vitelli, C.; Crespi, A.; Ramponi, R.; Osellame, R.; Mataloni, P.; Sciarrino, F. Quantum interferometry with three-dimensional geometry. *Sci. Rep.* **2012**, *2*, 862. [CrossRef]
41. Glauber, R.J. Coherent and incoherent states of the radiation field. *Phys. Rev.* **1963**, *131*, 2766–2788. [CrossRef]
42. Walls, D.F.; Milburn, G.J. *Quantum Optics*; Springer: Berlin/Heidelberg, Germany, 2008. [CrossRef]